UNIVERSITAT POLITÈCNICA DE CATALUNYA
BARCELONATECH
Escola d'Enginyeria de Telecomunicació i Aeroespacial de Castelldefels

Master's degree in Applications and Technologies for Unmanned Aircraft Systems

MASTER THESIS

TITLE: Underground inspection drone - case study in Barcelona sewage system

MASTER DEGREE: Master's degree in Applications and Technologies for Unmanned Aircraft Systems (Drones) (MED)

AUTHOR: Viet Vu Tran

ADVISOR: Jose Ignasio Rojas Gregorio

DATE: September, 3rd 2018

Abstract

Sewage system plays an important role in the infrastructure of cities like Barcelona and needs to be inspected and maintained on a regular basis in order to assure its good operation. The current walkthrough inspection method is tedious, unhealthy and dangerous. From this reality, it was proposed that an autonomous drone carrying needed sensors flies in the sewer and collects the data necessary for the inspection.

This thesis studies the integration of drone in the inspection operation of underground infrastructures with a focus on sewage system inspection, in the circumstances of Barcelona city. This study will concentrate on the range sensing methods, particularly range sensing using Lidar, which helps the drone navigate in a closed confined space and in the absence of GNSS navigation. This is crucial in order for the drone to avoid crashing on the walls of the sewer or on other obstacles and accomplish the mission. Several commercial rangefinder sensors are proposed for this project and a comparison is made under several criteria so as to select a best option for the application.

Furthermore, this study analyses the requirements for a drone platform conceived for the said application. The architecture of such platform is introduced and evaluated. The building of a practical unmanned aerial vehicle prototype able to perform the inspection is also presented. It was decided that an octocopter of coaxial configuration is the best option for the application, as it allows the platform to have the sufficient power for the application while maintaining its compactness and meanwhile increasing the redundancy and thus improving the security. Details of the key component used in the prototype are presented to give the reader a practical view about the prototype. The result was a prototype of drone platform whose first tests were conducted showing positive results.

CONTENTS

LIST OF FIGURES

LIST OF TABLES

INTRODUCTION

The objective of this thesis is to study the application of drone in underground inspection. In particular, it aims at the inspection of sewage system, in circumstances of a big city, taking Barcelona sewage as the object of the study. Barcelona sewage network is a wide and intricate network in which more than 1500 km of sewer is connected to carry both wastewater (sewage water) and rainwater (drainage water). Currently, inspection of this network is perform by inspecting staff using traditional walkthrough method. This method implies that the workers have to climb down the sewers by accessing via manholes and walk along the all the sewer to check the section needed to be inspected. This method of inspection is difficult, time-consuming and can be dangerous, hence not very efficient. Every year, around 1 million euros is needed in staff payment only for this work. The inefficiency and hazardous nature of the traditional method has motivated the application of new technologies to this inspection work, among which drone appears to be an appealing solution.

In order to achieve its goals, a set of tasks was set in this thesis, including:

- Study the sewage system of Barcelona, identify its problems concerning inspection
- Analyze the advantages and disadvantages of using drones in sewer inspection
- Study the Lidar technology in range sensing to apply in obstacle detection and avoidance
- Build a prototype capable of carrying 1100 gr payload with minimum 10 minutes of autonomy

This thesis is structured into three main parts, each one is covered in one chapter. The first chapter will study the actual problems of the sewage system with a focus on the sewers in Barcelona. It points out the necessity of a new technology to replace the current walk-through method, which is difficult, unhealthy and unsafe. The solution proposed is to use a drone platform that carries the cameras and sensors to replace human in inspection missions. This part also analyses the challenge such a technology should encounter and emphasizes the substantial benefits it would bring.

The second chapter focuses on range sensing technology, one essential subject that would decide the success or failure of the drone application. Due to the space constraints and the lack of GNSS navigation, the drone will have to rely on its own obstacle detection and avoidance capacity to fulfill the task. Lidar technology was proposed to solve this problem. Different rangefinder sensors were also compared and the one that fits the best the application was selected.

In the last chapter, this thesis introduces a drone platform built by the author, keeping in mind the requirements of the mission. Different key components were analyzed and real parts used in the drone were presented.

The thesis concludes by assuming the accomplishments of the study as well as the drawbacks where it can be improved, and proposes possible improvements for the future work.

Chapter 1: Problem description

1.1. Overview of sewer network and its problems

1.1.1. Sewer problems

Sewer network, although not quite visible in our daily lives, plays a crucial role in the infrastructure of any city. It conveys wastewater away from the population and drains the surface water, thus preventing flooding and the spreading of diseases. It is obvious that, the bigger a city is, the more important is its sewer network. For example, by the year 2006 the sewer network of Barcelona had expanded to about 1500 km and it serves a population of 1.7 million people as well as all commercial and industrial activities located in the city, with a considerable and increasing number of tourists [1].

The sewer system is subjected to obstruction from different origins. Particularly, with the quick growth of the population and the industry, the probability of blocking is higher. Also, the soil may collapse and reach the underground sewer network, especially in places where heavy transportation frequently crosses. Common problems that a sewer system may encounter are listed below [2].

- Cracked sewer walls and pipes: as sewer deteriorates with time, its wall and pipe may get cracked. This can also be triggered by earth movement.
- Misaligned and open pipe joints: this may be a construction error or a consequence of long time use. The mortar used to seal the joints between sections deteriorate with time, causing the joint to open and water to leak.
- Missing or unrecorded sewer pipes and manholes, inappropriate changes in the network. In Barcelona, the sewers date back from late 19th century with 'Garcia Faria Plan' and have undergone three main changes in the 20th centuries. The long use and changes may the origin of issues and problems.
- Overloaded sewer: new oversizing sewer construction, illegal connections and infiltrated water from ground or other sources may overload the current system.
- Defective manholes: typically manholes are in operative condition as they are more visited and easier to inspect. However manholes can be misaligned due to external impaction or deteriorate by the use.
- Flatten or leveled main/lateral sewer.

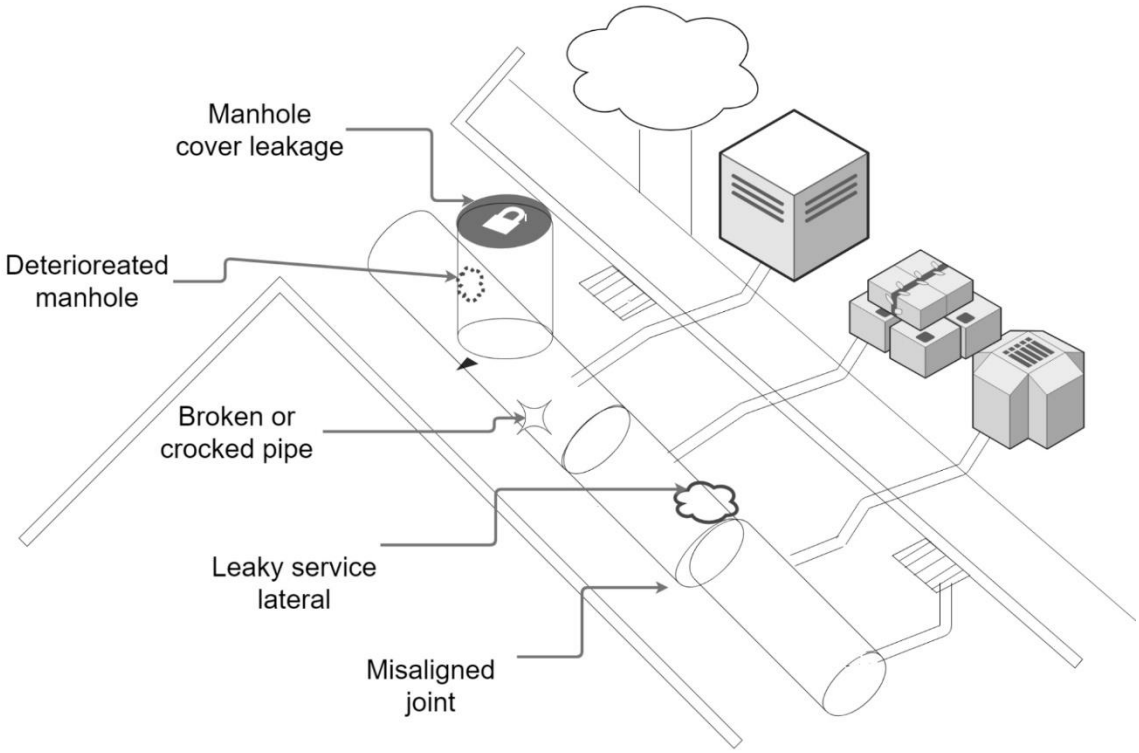

Fig. 1.1 Typical problems in sewer

The most concerned problem with a sewer is clogging or congestion. This happens when the flow if blocked and little or no flow can pass through. This may due to different reasons. Common causes include:

- Root infiltration: when the sealing of the sewer diminishes, the deep roots of the vegetation from above can infiltrate to feed on the water and thus create obstacles that prevent optimal flow. Tree roots are major cause of clog-up in sewer lateral where the sewer is near ground surface.
- Water infiltration: when large water flows infiltrate into the sewer (from storm, for instance), this causes overflows in the network. When the rain is very intense, an important quantity of water enters the drainage system, combined with the water infiltrating the soil; the water level can increase to such a high level that overpass the capacity of the drainage system.
- Solids build up: many types of solid materials (dirt, bones, tampons, paper towels, diapers, broken dishware, garbage, concrete, debris, etc.) may enter the sewer network and build up in the pipe causing stag. These accumulations do not allow the water circulate.
- Structural defects in pipes and manholes: cracks, holes, misaligned pipe, and offset joints are all possible causes of clogging.

1.1.2. Solution proposal

Frequent inspection of the inside of the sewer on a regular basis to detect problems before they results in failures. At present, the structural and operational condition of the sewers in Barcelona is checked manually by traditional walk-though method

performed by workers. This task requires the staff to work in confined space with extreme condition of humidity and temperature, and certain level of risk. Needless to say, the working condition of this inspection work is uncomfortable, unhealthy, difficult and not entirely safe.

To solve the problems related to the unfavourable environment in the sewer network, the idea of using automatic tools to replace human inspection work has been proposed. By the end of 2014, a pilot project was started within the framework of European Union's ECHORD++ innovation program to develop robots capable of carrying out the inspection work under the drainage and sewer network of Barcelona. If a satisfactory technological solution is found, it would be applied in other cities in Europe and worldwide [3].

1.2. Drone for sewer inspection

1.2.1. Challenges for sewer inspection using drone

The sewer network is a hostile environment. Although the corridors vary in sizes, they are in general small and narrow. Normally, the sewer has no source of illumination, the floor is normally wet and the sidewalks are slippery (see Figure 1.2). Almost all the network is completely dark, the atmosphere is highly humid and the air is smelly. Sometimes, there are even dangers of toxic gases. Approximately 70 percent of Barcelona sewer network can be entered. The accessible areas have a minimum height of 1.3 meters. Drones can be very helpful in serving as a tool to support people in problematic conditions such as entering places difficult for human to access or working in dangerous or toxic environment.

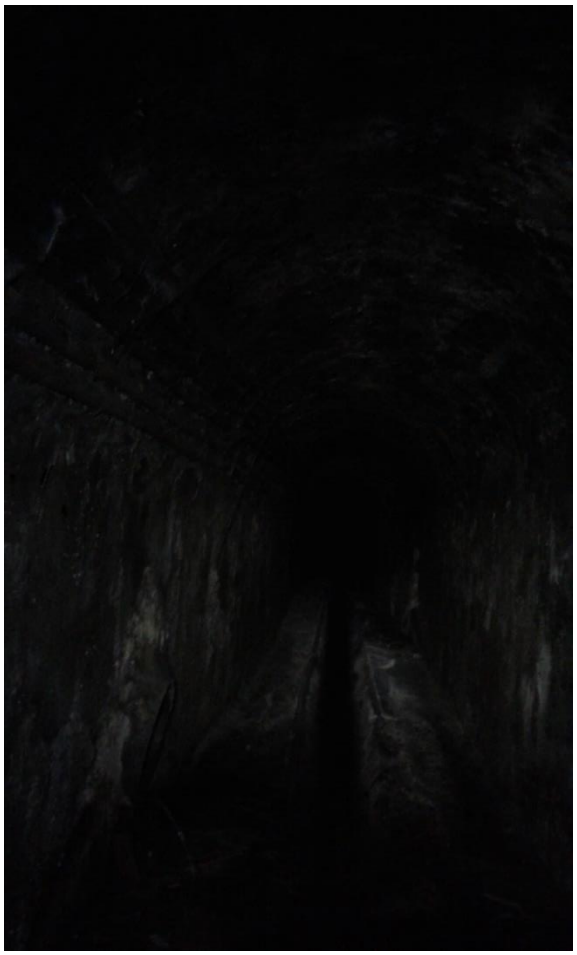

Fig. 1.2 Dark narrow corridor of sewer bellow Passeig de Gracia, Barcelona

Operating a drone in the sewer network implies different challenges. First and foremost, the underground surrounding restricts all the use of GNSS/GPS and other external positioning sources. As a consequence, the drones must calculate its position and speed all by itself, using the data it gets from the surroundings inside the sewer network. The drone needs to keep a safe distance from the solid walls, the ceiling and the water running underneath. This is a very challenging task, considering the narrowness of the sewer network and the little space for maneuvering. Besides, the total lack of illumination implies that the drone has to carry its own light sources if any photogrammetry is to be done. As the infrastructure degrades over the decades, the air blasts generated by the propellers will produce dust from mortar, a situation that the drone needs to be able to endure. Moreover, as the drone will be flying in an enclosed space, the propellers will create turbulence, and the drone should be able to maintain stable flight in these conditions.

1.2.2. Advantages of sewer inspection using drone

Despite all the challenges inspection of sewer using drone may face, there are many advantages that this technology conveys. Firstly, from the health and safety point of view, it reduces significantly the risk of working in hostile and dangerous environment. More importantly, the amount of information this technology produces considerably

superior to the traditional methods. This information is also easily stored and can be consulted in an objective manner during a long period of time. On the whole, this new technology allows accomplish inspection mission along the entire sewer length more rapidly, improving to a large extend productivity. The benefits this technology brings in risky situations are also of great importance. A sewer might collapse at some time, and it is of high interest to have a tool which can approach the zone to capture the situation on the field without putting any worker at risk. Eurecat's Robotics Unit director, Pepa Sedó estimates "a drone can inspect 300 meters in 10 minutes", meaning that a team operating one drone will be able to completely inspect 2.4 kilometers of the sewer network per day, "with a drastic reduction on costs and inconveniences".

It should be noted that, according to Barcelona Cicle de l'Aigua S.A. (BCASA) the current inspections rate is about 1.5 km of sewer every 6 hours, i.e. 2.0 kilometers per 8 hours of work. That would mean the drone would increase the rate of inspection by 20 percent while reducing the related labour. Taking into account that inspection activity costs Barcelona more than 1 million euros (staff roll alone is roughly 1 M€, as stated by BCASA), the economic potential gain of this application is high. Additionally, the underground inspection will be an ideal application for drones since it does not require the authorization of Spanish Aerial Navigation Authority AESA (Agencia Estatal de Seguridad Aérea) to fly.

1.3. Barcelona sewer network data

The sewer of Barcelona can be divided into three section categories (see Figure.1.3) depending on their sizes [4]:

- Non-accessible section (staff access is not allowed): diameter < 100 cm, or height < 50cm and width < 50 cm.
- Semi-accessible section (access is restricted to additional measure and is exclusive for particular tasks): diameter ≥ 100 cm, or height ≥ 100 cm and width ≥ 50 cm
- Accessible section (allows staffs to enter into its interior): diameter ≥ 150 cm, or height ≥ 150 cm and width ≥ 60 cm

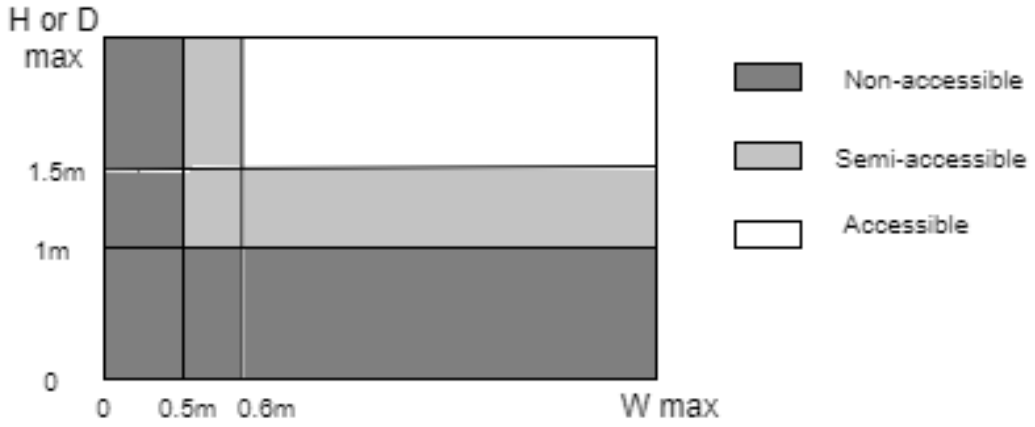

Fig. 1.3 Sewer section categories

The length of Barcelona sewer section categories is shown in the following table.

Table 1.1 Length of Barcelona sewer according to section categories

Section Category	Length (km)	Percentage
Non-accessible	541	35%
Semi-accessible	148	10%
Accessible	843	55%
Total	1532	100%

Table 1.2 shows the length of Barcelona sewer section according to ranges of height and type of section (tubular and non-tubular).

Table 1.2 Length of Barcelona sewer according to height and section type

Height	Non-tubular section length (km)	Tubular section length (km)
< 1.0 m	30	511
1.0 - 1.5m	114	34
1.5 - 2 m	668	6
2 - 2. 5 m	91	4
2.5 - 3 m	44	1
> 3 m	27	2
Total	974	558
	1532 km	

One important data of the sewer network for inspection mission is the cross section of the sewer. As mentioned previously, Barcelona sewer network has undergone many extension and renovation plans. As a consequence, the cross sections of the sewer vary a lot. There are 2076 different types of sections existing in the network. However, the two most common types are T111 and T120, which are shown in the figure below.

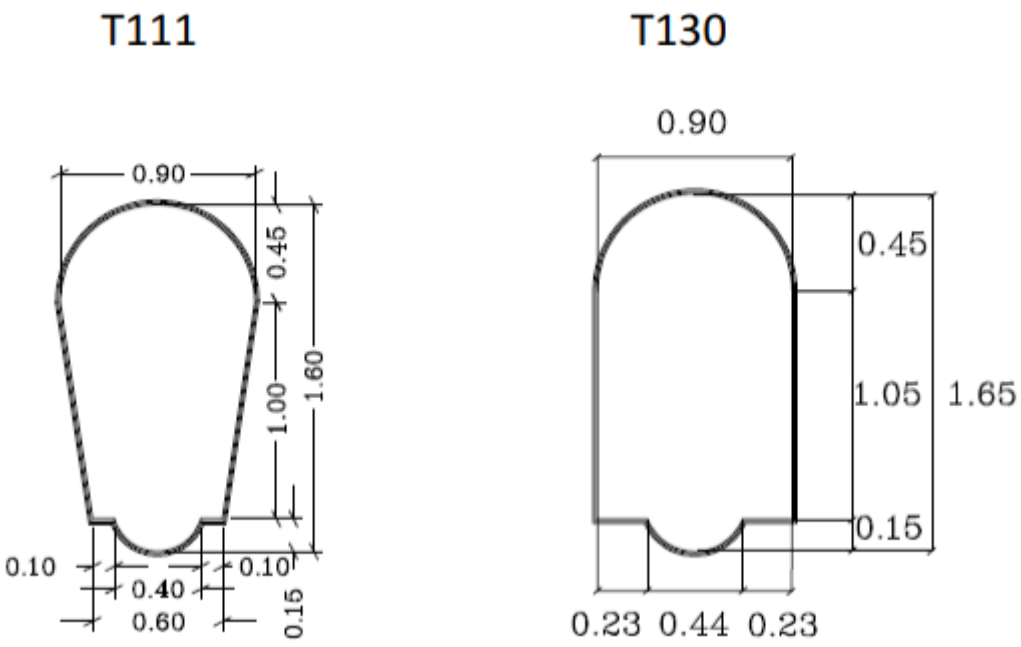

Fig. 1.4 Typical sections of Barcelona sewer

Image courtesy: BCASA

Chapter 2. Lidar sensor for range sensing

2.1. Lidar principle

2.1.1. Lidar description

Lidar, also written LiDAR or LIDAR, stands for Light Detection and Ranging. This is a remote sensing system using photon beams to measure the distance from the sensor to an obstacle by emitting the said photon beams to the target and analyzing the reflected beam. The name '' Light Detection and Ranging'' is rather misleading because the radiation used in this technology is not limited to the visible light range of the spectrum [5].

The photon beam employed in Lidar can be ultraviolet, visible light, or near infrared light, meaning that the wavelength can vary from 250 nanometers of UV light to 10 micrometers of infrared light, covering optical range of wavelength. Depending on the wavelength, the optimally detectable material also changes, but in general, a wide variety of targets can be detected, not only metallic materials but also non-metallic materials such as plastics, concrete, rocks and in some cases even single molecules [6].

The emission can be pulsed laser or continuous wave laser. Pulsed laser is used in pulsed Lidar (discrete Lidar) and continuous wave laser is used in continuous wave Lidar (full-waveform Lidar). In the former case, the energy transmitted is of short duration and the amplitude of the returning signal will be used to detect ranges; while in the latter case, the continuous wave laser detects ranges by analyzing the difference in phase between the transmitted and received signal [7]. The system onboard the platform emits light beams. When the light wave meets a surface, it reflects and comes back to the Lidar sensor. The sensors then measures these photons. From that and knowing the speed of lights, the distance to the object can be calculated. On that basis, Lidar can be used to collect data needed for detecting obstacles to navigation, and also for topographic mapping which is used to make a map or 3D image of the area of interest. The subsequent part will introduce the principle of Lidar remote sensing.

2.1.2. Principle of Lidar sensing

Lidar works on the principle of measuring the distance to an obstacle by calculating the traveling time between the emission of a signal and its return after hitting the object (Figure 2.1).

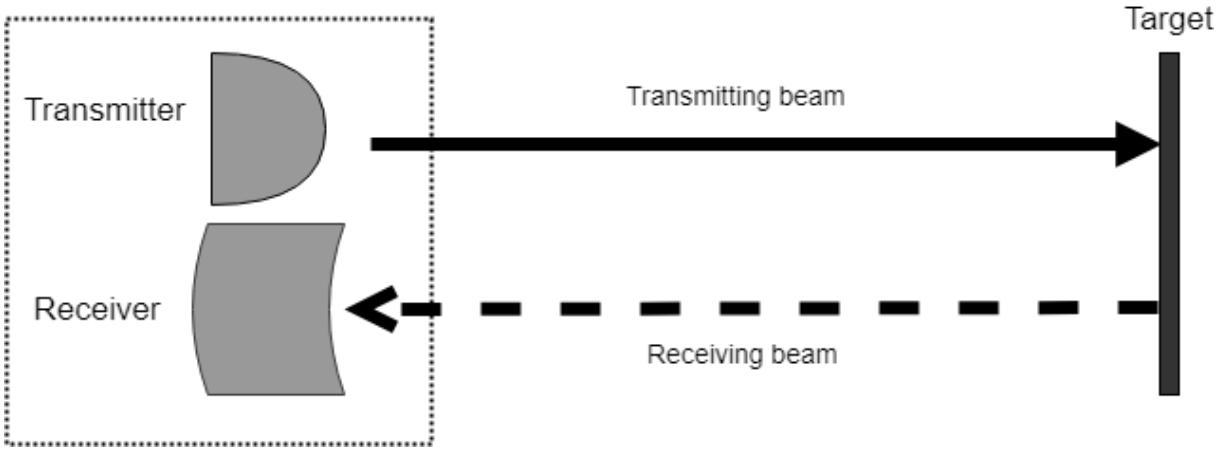

Fig. 2.1 Lidar range measurement operation

In the case of pulsed transmission, a beam (pulse) of light is emitted from the transmitter and the precise transmitting time is recorded. The beam then travels at light speed, reaches the object and reflects back home to contact with the receiver. At the receiver, the reflection of the beam is detected and the precise returning time is recorded. By subtracting the returning time by the transmitting time, the interval between two signals is calculated. This time interval allows to calculate the distance from the Lidar to the obstacle by the formula:

$$R = c\frac{t}{2} \tag{2.1}$$

Where:
R is the range distance
c is the speed of light (~299792458 m/s in standard atmosphere condition)
t is the time interval between transmitting and receiving signals.

The range resolution can be calculated by the following formula:

$$\Delta R = c\frac{\Delta t}{2} \tag{2.2}$$

Where ΔR and Δt are range resolution and resolution of time measurement.

Similarly, in the case of continuous phase-shift wave laser, the distance from Lidar sensor to the target is calculated by measuring the different if phase of the receiving and the transmitting signal. If the oscillator of the transmitter modulates the current of the laser generator (diode) by a frequency f, the formula to calculate range distance is the following:

$$R = \frac{c}{2}\frac{\varphi}{2\pi f} \tag{2.3}$$

Where:
φ is the phase shift, φ = 2πft
f is the frequency of the modulated wave.

The main components of a Lidar system are presented in the Figure 2.2.

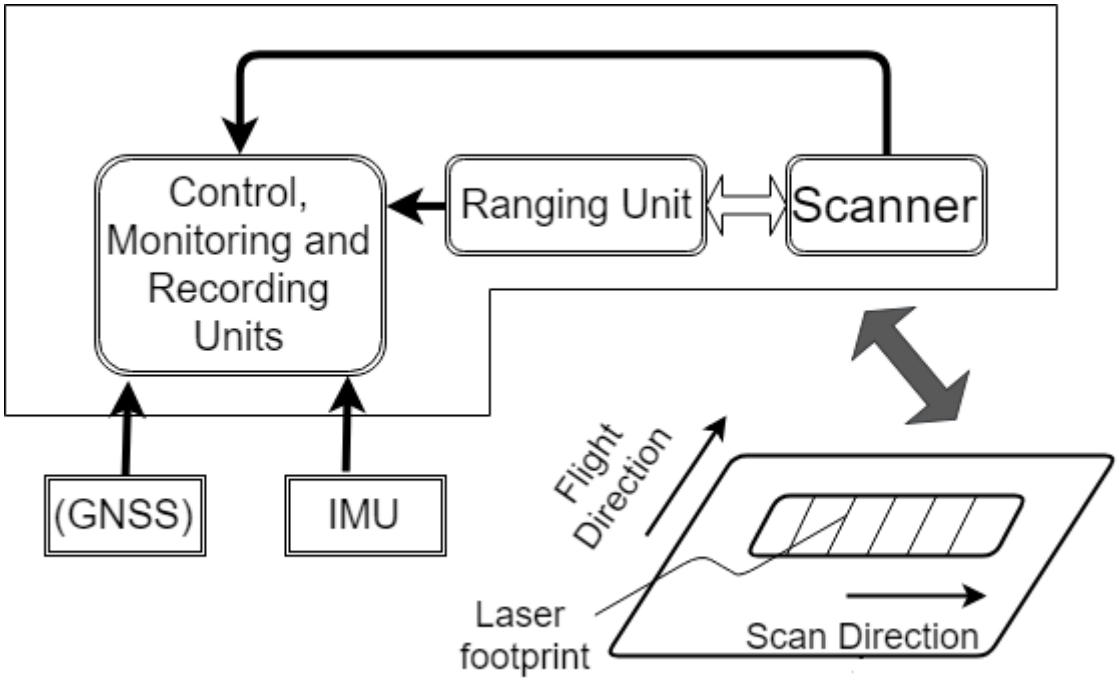

Fig. 2.2 Key components of a typical Lidar system

As it can be seen, a Lidar system consists of three main components: ranging unit, opto-mechanical scanner and control-processing unit [8].

The ranging unit includes a laser emitter and a receiver which are located at the same place in the system. They are arranged so that the paths of transmitting and receiving signal are on the same optical path so that the surface pointed on the object falls on the field of view of the receiver. Besides, the aperture of the receiver is normally higher than that of the transmitter. In a typical Lidar system for ground or aerial application, the Global Navigation Satellite System (GNSS) Unit and Inertial Measurement Unit (IMU) comprise the Position and Orientation System (POS). The application in this study excludes the use of GNSS, for that reason position and orientation will be provided only by IMU onboard. Ideally, the IMU unit should be placed as close to the scanner as possible to record the orientation and aircraft vibration at the location of the Lidar. Typically, the instantaneous field of view (IFOV) of the emitting beam and the receiving beam is small, ranging from 0.3 milliradian to 2 milliradian. To obtain surface coverage, the transmitting and receiving beams need to sweep across the flight line. This is obtained by an opto-mechanical scanner. The scanner may use two rotating prisms (refraction scanner) or rotating/oscillating mirrors (reflection scanner) [9]. Fiber scanning technology can also be employed but not very commonly. As it can be observed in the Figure.2.2, Control, Monitoring and Recording Units are in the central position of a Lidar system. Their function is to synchronize the Ranging Unit with the scanner, trigger the transmitting signal synchronously with the incremental scanner

steps, and store the ranging dataset into memory device. The data includes slant ranges of the returning signal, the returning signal intensity, the instantaneous scanning angles and high precision time stamps.

One important application of Lidar is in 3D mapping applications [10]. Topographic Lidar uses a series of measured distance to obstacles, combined with the location (position and orientation) of the platform to generate a three dimensional scene of the surroundings [11]. Generally, this scene is formed by a point cloud of series of 3D coordinates stored in the platform's memory device. A high resolution point cloud of physical features can be obtained by a narrow beam.

This study will not examine the topographic application of Lidar but focuses on the range detection application, which will be discussed in details in the subsequent part.

2.2. Rangefinder sensor

2.2.1. Range sensing problem

In this study, a particular problem of indoor geo-localization has been raised for the application of interest. In order to implement the tasks in underground environment, the drone platform needs to be able to perform obstacle detection and avoidance. This can be done by means of rangefinder sensors using Lidar or ultrasound technology.

The drone platform is designed to flight in a highly restricted three-dimensional space, which requires measurements and tracking of small movements. This implies that, for the rangefinder onboard the drone platform, a high measurement rate for a point should be of greater importance than a bigger number of points at lower rate. Besides, the stability of the measurement needs to be prioritized otherwise the platform can crush easily once the sensor gets a hitch. This is the reason why ultrasound sensors, which frequently have big jumps in reading even at constant distance to a target, are not preferred, and the Lidar rangefinders are of great interest in this study. Additionally, the high stability requirement entails the need of filtering out-of-range values, leading to a slower refresh rate.

2.2.2. Four rangefinder sensors under consideration

A group of researchers have conducted experiments [12] in underground scientific tunnel facilities of European Organization for Nuclear Research (CERN) in order to compare different range finder sensors of similar scope. The result of these experiments are presented in the subsequent section.

Four rangefinder sensors based on different technologies were compared. They are listed below (Figure 2.3).

- XL MaxSonar EZ Series MB1200 from MaxBotix using ultrasonic range finder technology [13]
- SF01 INT from LightWare Optoelectronics using Laser or Lidar [14]
- UTM 30LX from Hokuyo Automatic Co. using Lidar [15]

- TeraRanger One (TR One) from Terabee using Timeof-Flight IR LED (similar to Lidar) [16]

Fig. 2.3 Four rangefinders of interest. From left to right: MB1200, SF01 INT, UTM 30XL, TeraRanger

The specifications from the four manufacturers are compared in the following table.

Table 2.1 Specification of four rangefinders of interest

	MB1200	**SF01 INT**	**UTM 30XL**	**TeraRanger**
Resolution (cm)	1.0	1.0	1.0-10.0	0.5
Current requirement (mA)	3-4	150	700-1000	50-150
Voltage requirement (VDC)	5.9	205	370	203.3-5.5
Weight (gr)	3.3-5.5	4.5-5.5	10.8-13.2	10-20
Dimension (mm)	20x20x25	60x52x155	60x60x87	32x27x15
Maximum range (m)	7.65	60	30	14
Operating temperature (ºC)	0-65	-10-50	-10-50	-10-50
Measurement rate (Hz)	10	8	40	1000
Approximate price (Euros)	40	480	4100	125

Experiments have been carried out to demonstrate different properties of the four rangefinders in practical condition of underground tunnel facilities. Five parameters representing a standard sensor are taken into account, including: non-linearity, resolution, accuracy and precision. In each experiments, the TeraRanger sensor is tested in both Speed Mode (SP) and Precision Mode (PM). The former mode is designed for collision avoidance thus precision is not a priority; while the latter mode

aims at navigation hence the precision and accuracy are more important. The results of the previously mentioned researches are introduced subsequently.

2.3. Comparison of the four rangefinder sensors proposed

2.3.1. Comparison of non-linearity

The first parameter to compare among four rangefinders is non-linearity. This parameter shows the dissimilarity between experimental measurements of the sensors and a reference value measured by a high precision meter, by calculating the maximum deviation from a first polynomial fit. Non-linearity is the least significant of all the errors in a sensor. The non-linearity results are shown and compared in the following table:

Table 2.2 Result of non-linearity of four rangefinders (TeraRanger in two modes)

	MB1200	SF01 INT	UTM 30XL	TeraRanger PM	TeraRanger SM
Non-linearity (%)	1.33	0.34	0.25	0.29	4.16

It can be observed that UTM 30XL has the best linearity result while TeraRanger in Speed Mode exhibits highest non-linearity. However, in Precision Mode, TeraRanger shows great improvement of linearity results.

2.3.2. Comparison of resolution

Secondly, the resolution of four sensors are tested. Precision of the rangefinders are defined as the smallest displacement change that the sensor can detect. The test is carried out at seven different distance ranges. It should be noted that the MB1200 ultrasonic rangefinder and the Speed Mode of TeraRanger are designed to work at short ranges, thus the tests for those cases are limited to 0.5 meters. The results of resolution are shown in the tables below.

Table 2.3 Result of resolution (in cm) of four rangefinders

Range (cm)	MB1200	SF01 INT	UTM 30XL	TeraRanger PM	TeraRanger SM
50	1.0 cm	0.5 cm	1.0 cm	0.5 cm	>5
100	1.0 cm	0.5 cm	1.0 cm	0.5 cm	>5
300	1.0 cm	0.5 cm	1.0 cm	0.5 cm	>5
500	1.0 cm	0.5 cm	1.0 cm	0.5 cm	Out of range
800	Out of range	1.0 cm	1.0 cm	1.0 cm	Out of range
1000	Out of range	1.0 cm	2.0 cm	1.0 cm	Out of range
1300	Out of range	1.0 cm	2.0 cm	1.0 cm	Out of range

Table 2.4 Result of resolution (in % range) of four rangefinders

Range (cm)	MB1200	SF01 INT	UTM 30XL	TeraRanger PM	TeraRanger SM
50	2.00 %	1.00 %	2.00 %	1.00 %	>10.00 %
100	1.00 %	0.50 %	1.00 %	0.5 %	>5.00 %
300	0.33 %	0.17 %	0.33 %	0.17 %	>1.67 %
500	0.20 %	0.10 %	0.20 %	0.10 %	Out of range
800	Out of range	0.13 %	0.13 %	0.13 %	Out of range
1000	Out of range	0.10 %	0.20 %	0.10 %	Out of range
1300	Out of range	0.08 %	0.15 %	0.08 %	Out of range

It can be seen that the MB1200 sensor's resolution is maintained at 1.0 cm in the short range tested. Both SF01 INT sensor and TeraRanger sensor in Precision Mode have good resolution at ranges under 500 cm. The TeraRanger in Speed Mode has unsurprisingly bad resolution in the tested range.

2.3.3. Comparison of accuracy

Thirdly, the accuracy of the four rangefinders was put in question. This parameter represents the maximum deviation of the displacement measured by the sensor in comparison with the reference value. To calculate accuracy of each rangefinder, 400 measurement values were read at each range. The accuracy result is shown in the tables below.

Table 2.5 Result of accuracy (in cm) of four rangefinders

Range (cm)	MB1200	SF01 INT	UTM 30XL	TeraRanger PM	TeraRanger SM
50	5.0 cm	1.0 cm	1.0 cm	2.0 cm	2.0 cm
100	6.0 cm	2.0 cm	1.0 cm	2.0 cm	3.5 cm
300	8.0 cm	1.3 cm	2.0 cm	2.0 cm	>10
500	9.0 cm	2.0 cm	2.0 cm	2.2 cm	>10 cm
800	Out of range	1.5 cm	2.0 cm	2.2 cm	Out of range
1000	Out of range	2.0 cm	2.0 cm	2.3 cm	Out of range
1300	Out of range	3.0 cm	3.0 cm	3.2 cm	Out of range

Table 2.6 Result of accuracy (in % range) of four rangefinders

Range (cm)	MB1200	SF01 INT	UTM 30XL	TeraRanger PM	TeraRanger SM
50	10.00 %	2.00 %	2.00 %	1.00 %	4.00 %
100	6.00 %	2.00 %	1.00 %	2.00	3.50 %
300	2.67 %	0.43 %	0.67 %	0.67 %	3.33 %
500	1.80 %	0.40 %	0.40 %	0.44 %	2.00 %
800	Out of range	0.19 %	0.25 %	0.28 %	Out of range
1000	Out of range	0.20 %	0.20 %	0.23 %	Out of range
1300	Out of range	0.23 %	0.23 %	0.25 %	Out of range

The results show that the MB1200 sensor has lowest accuracy and its accuracy decreases rapidly when the range increases. The SF01 INT sensor has good accuracy in general, yet this quality is not stable when the range changes. The UTM 30XL sensor exhibits the best accuracy and its accuracy slowly decreases when the range increases. In Precision Mode, the TeraRanger sensor has rather good accuracy, which also decreases gradually as the range increases. In Speed Mode, the TeraRanger sensor has fairly good accuracy at close range but loses this feature when the range exceeds 300cm.

2.3.4. Comparison of precision

The next parameter to compare is precision. It is the standard deviation of repeated measurements. The precision of four sensors are calculated after carrying out 400 displacement measurements at each range. The standard deviation result is given in the following table.

Table 2.7 Result of standard deviation (in cm) of four rangefinders

Range (cm)	MB1200	SF01 INT	UTM 30XL	TeraRanger PM	TeraRanger SM
50	0	0.44	0.52	0.58	0.43
100	0	0.45	0.48	0.49	1.17
300	0	0.43	0.48	0.74	8.14
500	0	0.46	0.52	0.83	23.51
800	Out of range	0.49	0.64	0.92	Out of range
1000	Out of range	0.53	0.68	0.81	Out of range
1300	Out of range	0.68	0.74	1.13	Out of range

The MB1200 sensor, although has low accuracy as stated in the previous analysis, has shown very good precision in the tested range. The SF01 INT sensor, the UTM 30XL sensor and the TeraRanger sensor in Precision Mode all show comparable and high accuracy. Similarly to the accuracy result, the TeraRanger sensor in Speed Mode has rather good accuracy at close range and low accuracy outside the range of 300 cm.

2.3.5. Comparison of update rate

Lastly, the refresh rate of the four sensors are compared. It indicates the number of effective measurements carried out in one second. This parameter is measured by counting the total returning values in a constant time interval which was set to 60 seconds then divide the number obtained by the set time interval. It is extremely important that the sensor has high rate in order to fulfill the requirement of the application in this study. The real valid rate results are shown in the table below.

Table 2.8 Result of update rate (Hz) of four rangefinders

Range (cm)	MB1200	SF01 INT	UTM 30XL	TeraRanger PM	TeraRanger SM
50	9.8	7.6	39.7	514.9	1046.5
100	9.9	7.9	39.8	444.5	1046.7
300	9.8	7.9	39.9	194.2	1047.9
500	9.9	7.9	39.9	66.3	1049.3
800	Out of range	7.9	39.9	18.2	Out of range
1000	Out of range	7.8	39.9	9.3	Out of range
1300	Out of range	7.9	39.9	4.6	Out of range

In order to highlight the difference among the update rates of the four sensors, Figure. 2.4 plots the result of update rate of all the cases against measurement range.

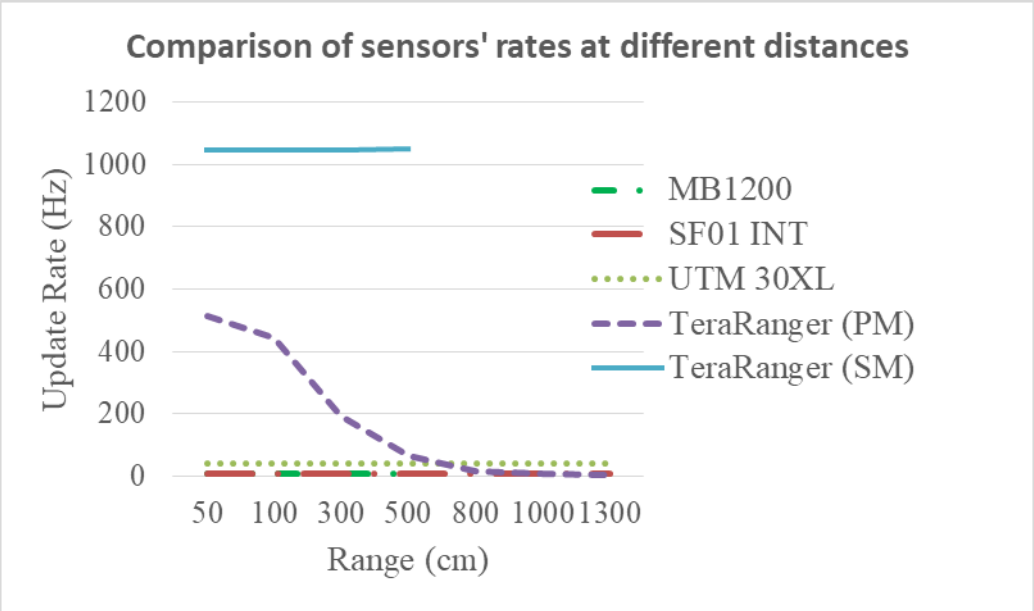

Fig. 2.4 Comparison of update rates of four sensors at different ranges

The results show that both the MB1200 sensor and SF01 INT have very low update rates. The UTM 30XL sensor has slightly higher rate; and, similarly to two former sensors, its refresh rate is kept constant, independently of the measuring distance. The TeraRanger sensor, on the other hand, has particularly high refresh rate at low range. When working in Precision Mode, the refresh rate of this sensor drops rapidly when

the distance increases. On the contrary, when the TeraRanger sensor works on Speed Mode, its refresh rate remains steadily high in all the tested range.

2.4. Conclusion on rangefinder selection

The previous evaluation has studied and compared the key parameters of the four rangefinders, taking into account both working modes of the TeraRanger rangefinder from Terabee. After analyzing the good points and drawbacks of all the rangefinders, TeraRanger One sensor from Terabee was selected for this study because of its small size, lightweight, high-performance distance measurement and most importantly high rate.

The update rate declared by the manufacturer Terabee is >1000Hz in Speed Mode, which is very important to the application. In spite of the fact that TeraRanger One sensor's strong points are only noticeable at close range, this does not prevent the application of interest in this study from benefiting from the advantages. This is due to the limited space in the underground infrastructures, where long-range sensor would become superfluous and unnecessary. All in all, TeraRanger One sensor would make a good rangefinder that fits the requirements of the application in this study.

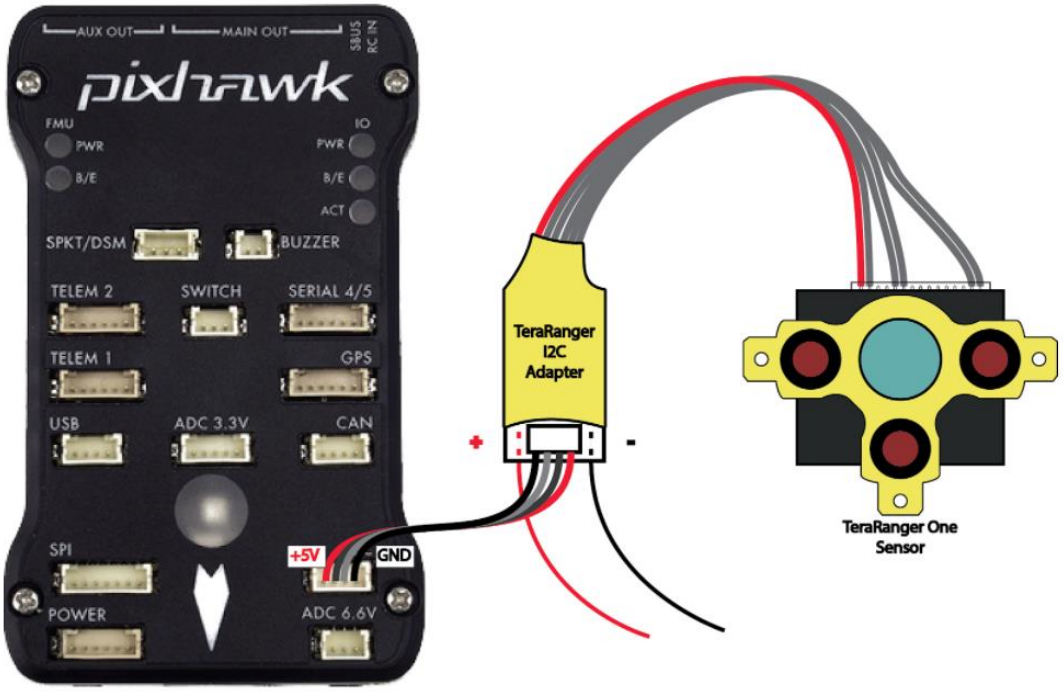

Fig. 2.5 TeraRanger One connected to Pixhawk autopilots

Image credit: Terabee.com, Published March 2018

The details on how to connect the TeraRanger One rangefinder to the flight controller of the drone platform (Figure. 2.5) as well as how to setup this rangefinder can be found in the Annex.

Chapter 3: Drone platform

In this part of the study, we will discuss the drone platform with its main subsystems; and describe a prototype (Figure.3.1) built by the author and colleagues from Flyscan Barcelona S.L. at IndronePark Barcelona.
The prototype was built having in mind the following requirements:

- Width and length shall not exceed 60 cm
- Autonomy (endurance) shall be over 10 minutes

The details of the architecture of this platform and its main components will be introduced in the subsequent sections.

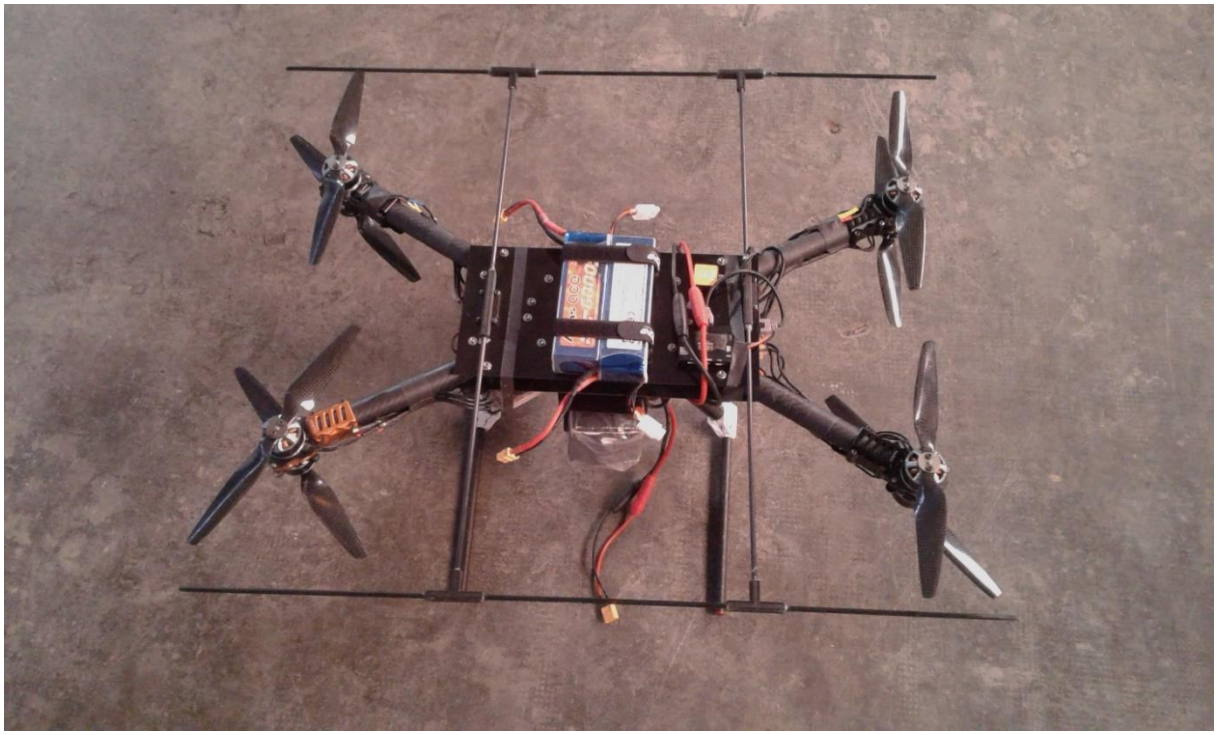

Fig. 3.1 Drone platform built during the project

3.1. Drone system architecture

The conceptual architecture of the drone system in this study can be perceived in the Figure. 3.2.

In this system, base station plays more a role of a monitoring station than of a control station. As the drone platform should flight autonomously, following the predefined flight plan, the operating team needs only to intervene in case of emergency, or if they spot interesting/alarming incidents and want to put the drone to a halt during flight plan. The base station features a graphical user interface (GUI) for the user to perform the intervention needed. Both the base station computer and control & communication unit

are powered by the battery carried on the truck, which also transports the drone platform and all related equipment to the inspection site. The drone platform and the base station are connected by means of WiFi connection via a WiFi relay that is dropped down the sewer by a cable. Thanks to that connection, the user can follow the operation on the camera and make adequate decision if necessary. The communication system is beyond the scope of this study, thus will not be discussed further.

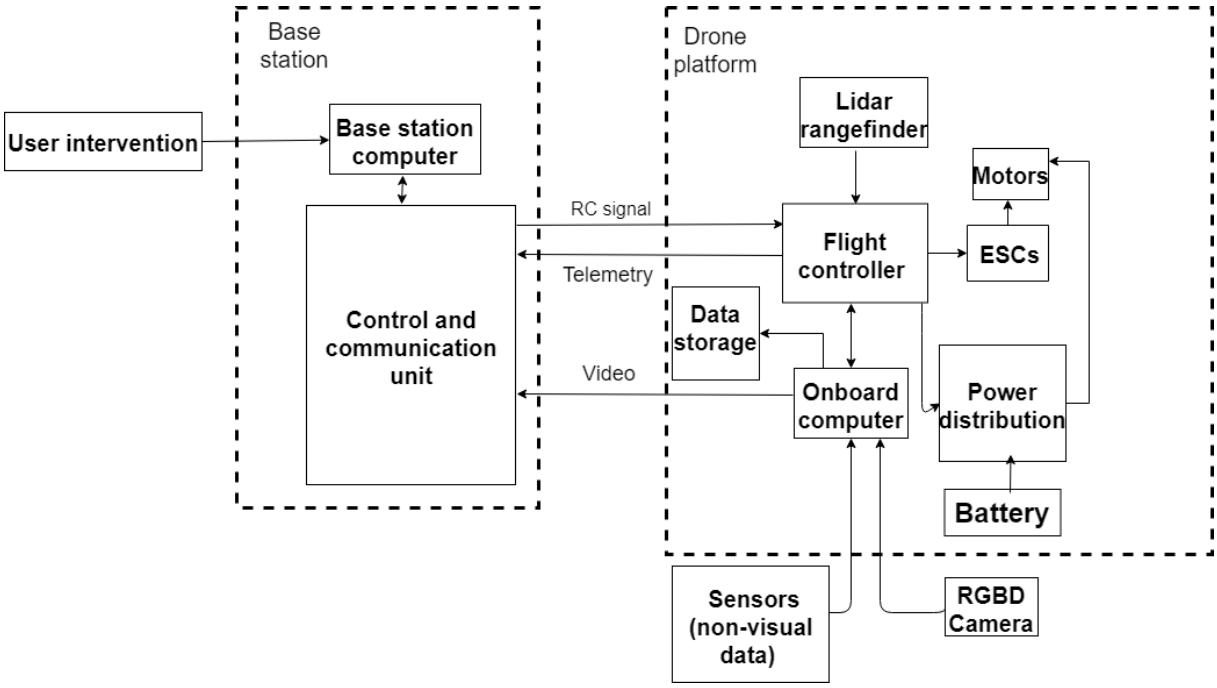

Fig. 3.2 Architecture of the drone system

In the drone platform, flight controller plays a central role. The platform uses flight controller for its open-source feature, high capacity and popularity. Details of the flight controller will be discussed latter.

As discussed before, navigation by GNSS in sewer is not a possible solution. Therefore, the drone will need to navigate using its IMU (inertial measurement unit) with the help of Lidar rangefinder for obstacle detection and avoidance. The details about range sensing can be found previously on Chapter 2.

The visual 3D camera (RGBD) and different types of sensors (gas sensors, thermal sensor) are the payloads of the system whose function is to collect the data needed for the inspection. Despite of their important roles, their details are beyond the scope of this study and should be investigated separately. The drone platform carries a computer onboard of type Raspberry Pi that preprocesses the information collected from the payloads and stores it to a memory device.

3.2. Coaxial octocopter configuration

Nowadays, there are many types of drone available, each one has various configurations of its own. Fixed wing aircrafts, helicopters and balloon-type drones are in general more corresponded to applications in larger space than in constrained environment like sewer. Therefore, it is obvious that, comparing with other different types of drone the multirotor configuration suits the application the best.

At the beginning of this study, a quadcopter configuration was selected. However, after the test, this configuration did not provide the necessary lift as required for this application. As a result, it was decided that the drone platform will use coaxial octocopter configuration (Figure. 3.3 and Figure. 3.4).

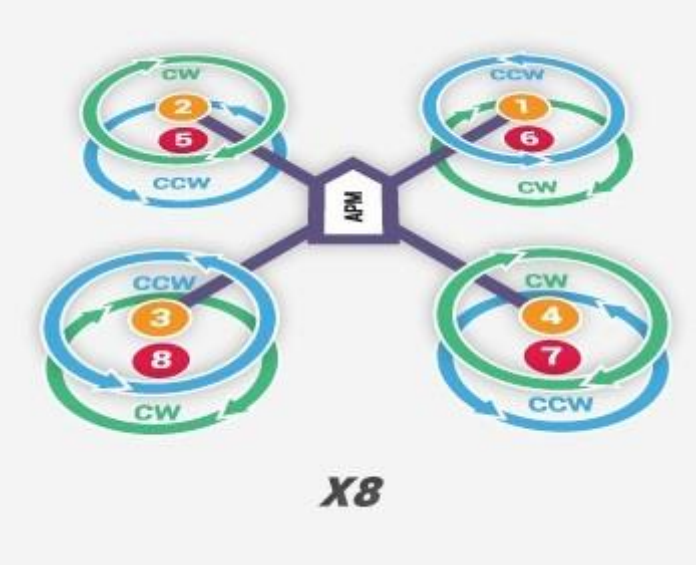

Fig. 3.3 Coaxial octocopter configuration
Image courtesy: Oscar Liang, "Types of multirotor" [16]

Fig. 3.4 Two motors mounted in coaxial configuration

Although the coaxial configuration implies 20-30% power loss when compared to separate propellers [17], the total lift of the drone is much higher than that of the quadcopter configuration while conserving its simplicity. One additional benefit of this configuration is higher redundancy: when one or more motors or propellers fail, the drone can still maintain the flight and have higher chances of accomplishing the mission or at least have a safe landing.

3.3. Flight/Power Subsystem

In this part of the study, the electrical and mechanical components that allow the drone flight will be analyzed and actual components that comprise the prototype will be presented.

3.3.1. Flight Controller

The flight controller or autopilot is usually considered the brain of a drone as it is responsible for the behavior of the drone during all the flight. It makes the drone platform flight by giving command signals to the Electronic Speed Controllers (ESCs) and by doing so, controls the motors. This project uses Pixhawk PX4 flight controller (Figure. 3.5), an open source autopilot that supports different kinds of drones, including fixed wing aircraft, multirotor, helicopter and even ground vehicles or water vehicle. It uses 168 MHz Cortex CPU and a 256kB RAM. It also features different types of sensors, including 3D accelerometer, gyroscope, barometer, and magnetometer.

Pixhawk flight controller was chosen over other flight controllers because of several reasons. There are various commercial flight controllers available such as DJI Wooking M, Mikrokopter or Hoverfly Pro. But those are closed-source flight controllers and have low programmability, which make them unfit for the project. Among the open-source flight controller, Pixhawk has rather higher memory and processing power when compared to others. This allows the flight controller to support the operation requirements without the risk of being overloaded. Moreover, the popularity of Pixhawk makes it a reasonable choice.

Fig. 3.5 Pixhawk PX4 flight controller and its top connectors

Image courtesy: Ardupilot.org

Pixhawk supports both PX4 and ArduPilot flight stacks. PX4 was chosen because it uses BSD license instead of GPL (GNU) license like ArduPilot flight stack. BSD open-source license allows the commercialization of the product and suits better the strategy of the company.

3.3.2. External IMU

Although Pixhawk flight controller has its own IMU, to increase the reliability of the system the drone is equipped with an external IMU unit. MTi 10-series IMU unit (Figure. 3.6) with 10 kHz simultaneous sampling rate is selected for the drone. It will provide extra navigation capability which is crucial for the application. This IMU is equipped with magnetometer yet this later will not be used for the application of this study.

Fig. 3.6 MTi 10-series IMU unit

Image courtesy: Xsens, MTi 10-series manual

The specification of the IMU can be seen in Table 3.1 and Table 3.2

Table 3.1 MTi 10-series inertial measurement unit system specifications

Input voltage	4.5 to 34V
Typical power Consumption	550 mW at 5V
IP-rating	IP67
Operation Temperature	-40 to 85 ºC
Casing material	Anodized aluminum 6082
Sampling frequency	10 kHz/channel (60 kS/s)
Clock drift	10 ppm or external reference
Output frequency	Up to 2 kHz
Interfaces	RS232/RS422/RS485/USB/UART (compatible to Pixhawk flight controller)
Latency	<2 ms
Sync options	SyncIn, SyncOut, Clock sync
Interface protocol	Xbus or ASCII (NMEA)
Mounting orientation	No restriction, full 360º in all axes
Built-in self test (BIT)	Gyroscopes, accelerometers, magnetometer
Mean Time Between Failures	300,000 hours

Table 3.2 MTi 10-series inertial measurement unit sensor specifications

	Gyroscopes	Accelerometers
Standard full range	+/- 450 º/s	+/- 20 g
Initial bias error	0.2 º/s	5 mg
In-run bias stability	18 º/h	15 µg
Bandwidth (-3 dB)	415 Hz	375 Hz
Noise density	0.03 º/s/√Hz	60 µg/√Hz
g-sensitivity (calibrated)	0.006 º/s/g	N/A
Non-orthogonality	0.05 deg	0.05 deg
Non-linearity	0.03%	0.1%

3.3.3. Motors and propeller

The drone uses eight brushless DC of type MN3110-17 700kv from Tmotors (Figure. 3.7) and 10"x4.5" carbon fiber propeller from Lumenier (Figure. 3.8).

Fig. 3.7 Tmotor MN3110-17 700kv

Image courtesy: Getfpv.com

Fig. 3.8 Lumenier 10x4.5 carbon fiber propellers

Image courtesy: Getfpv.com

The specifications of the T-motor is given in the table below (from Getfpv.com).

Table 3.3 T-motor MN3110-17 specifications

KV	700
Configuration	12N14P
Stator Diameter	31mm
Stator Length	10mm
Shaft Diameter	4mm
Motor Dimension(Dia.*Len)	Φ37.7×28.5mm
Weight(g)	80g
ldle current(10)@10v(A)	0.3A
No.of Cells(Lipo)	3-6S
Max Continuous current(A)180S	21A
Max Continuous Power(W)180S	466W
Max. efficiency current	(3-10A) >80%
Internal resistance	92mΩ

This propulsion system was tested and had proved to provide enough lift for the platform and its payloads.

3.3.4. Electronic Speed Controllers (ESCs)

ESCs output three-phase power to the motors and cause them to rotate. The speed of the motors is controlled by the pulse-width modulation (PWM) signal from the ESCs. The power supplied is proportional to its control input. It should be noted that the three-

phase power generated is not alternating current (AC) but direct current (DC) since the voltage of this power does not alter to negative but only change between zero and a peak value. In this project, 8 ESC of type KW60E / T60A from Kopterworx are used (Figure. 3.9).

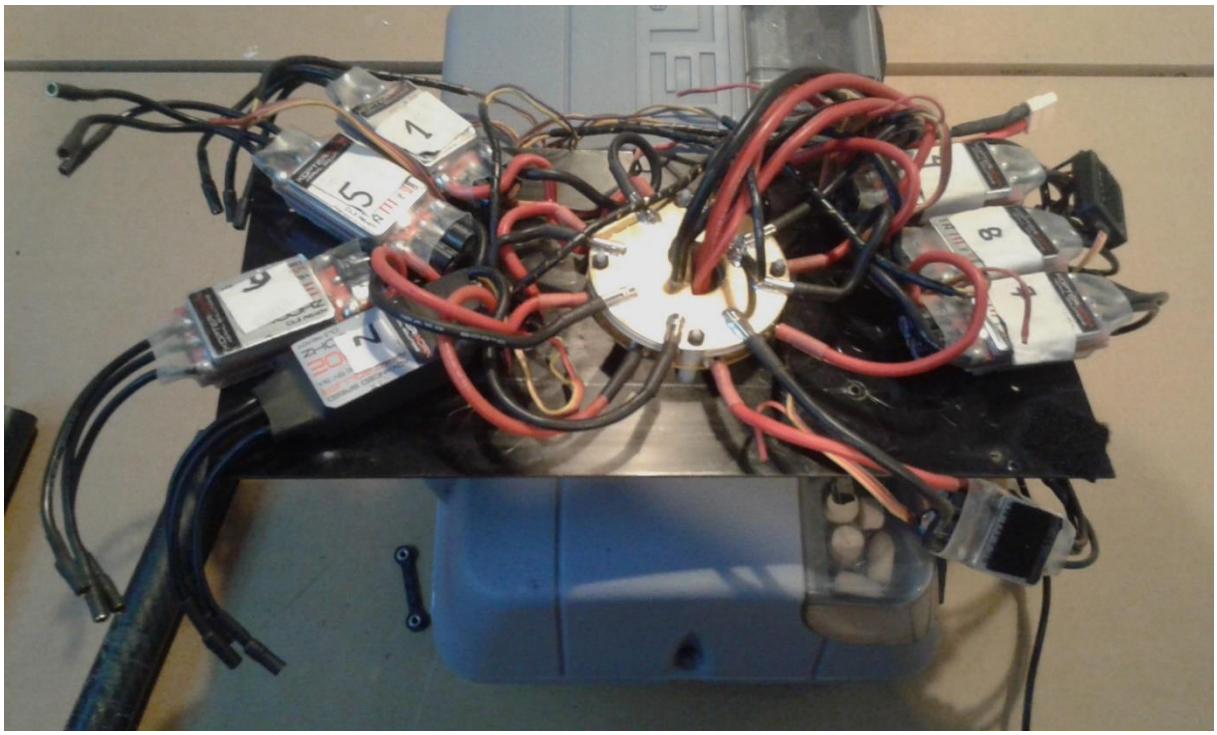

Fig. 3.9 Eight ESCs mounted on the central frame

3.3.5. Frame

A handmade frame of carbon fiber was made for the prototype in this study. It consists of a sandwich-type center module (Figure. 3.10) where flight controller, power distribution board, ESCs and batteries are mounted; and four extended arms (Figure. 3.11) to which the eight motors are attached (two motors on each arm. Besides, the frame also has simple carbon fiber bars to prevent the propellers from touching the obstacles (Figure. 3.1).

The lower part of the center module was cut from a plate of 1.5mm-thick carbon fiber. On this plate, eight plastic fixing rings were screw-mounted to support the four arms of the octocopter. Besides, power distribution disk and ESCs, are also fixed on this plate by double sided tape and screws, respectively. A landing gear made from carbon fiber tubes with 3D-printed joints was also added to the lower plate and was fixed by screws. The carbon fiber arms are made of 2mm-thick carbon fiber tubes. After the he tubes were cut; one of their ends, holes were drilled in order that they can be fixed on the center board, and on the other ends, mounting frames were fixed to mount the coaxial motors. The upper part of center module is an identical carbon fiber plate. The two plates are separated by metal separator on which skews were fixed on both sides to

connect the plates. On the upper plate, Velcro straps are added collocate the batteries which lay on top of the platform.

Fig. 3.10 Carbon fiber frame - center part with fixing rings for arms mounting

Fig. 3.11 Carbon fiber arms

Although the frame serves well its function of providing mechanical support for the components, it is not very aesthetically attractive and can be improved to protect the components better from water and dust.

3.3.6. Batteries

Lithium-Ion polymer (LiPo) batteries have become a standard for multirotor power source and this study is not an exception. Two LiPo 6000mAh 4S 35C 14.8V (Figure. 3.12) connected in parallel were used in this project. This provides a flying time of approximately 11.5 minutes when the platform carries 1100 gr of payload.

Fig. 3.12 Battery LiPo 6000mAh 4S 35C 14.8V

3.4. Final prototype

The prototype (see Figure. 3.1) measures 55cm by 58cm (from the tips of the propellers) and weights 3790 grams. After being built, it was put inside the sewer of Barcelona for autonomy test (Figure 3.13). With the setting described above, it has approximately 11 minutes and 30 seconds of flight time until the batteries level drops to 20 percent, while carrying 1100 grams of payload.

Fig. 3.13 Final prototype put in to test under sewer of Barcelona

3.5. Drone inspection operation

This part describes the operation of an inspection activity. The first stage of an operation begins with the planning of the inspection routes. After that, the flight plan is loaded to the drone which in turn is carried by a truck with the equipment needed to the inspection site. On the inspection site, the drone is lowered with the communication item down to the sewer through a manhole (Figure 3.14).

Once the platform is inside the sewer, the flight is executed and the drone carries out the preloaded flight plan. Even though the drone flights autonomously, the communication hub will allow the team on ground to monitor the flight and intervene when needed such as when to pause to make specific observations or in case of unexpected events. The flight leg ends when the drone lands at the point designated previously in the flight plan, which can be the same manhole where it began the flight or another manhole of the network.

Fig. 3.14 The drone prototype ready to be lowered down to the sewer

By the end of one leg, the team may change the battery or the flash memory to continue the inspection or recover the drone back on ground to take it to another inspection point, or else ends the flight, accordingly to the flight plan. When the flight plan is finished, the flash memory is taken from the platform and brought to an information center where the data will be analyzed in detail.

Conclusion

Concluding remarks

In this thesis, the problem of sewage inspection was raised and the solution using drone for this type of inspection was studied. It has analyzed the Barcelona sewage system and points out the limits of the current inspection methods as well as the potential of the new method using drone. When the problem was addressed and the solution proposed, this thesis has outlined the possible advantages of the new technology, not forgetting the challenges it may face.

To deal with the difficulty of flying a drone in the constrained space and lack of GNSS navigation, this thesis has highlighted the importance of using adequate range sensing technology. It also compared different types of rangefinder sensors to opt for the most suitable for this application. Finally, TeraRanger One sensor from Terabee was selected due to its good performance, especially in terms of update rate, accuracy and precision in close range.

This thesis has also examined the design of a drone system with monitoring base station and explained why the system is suitable for the mission. A practical platform with coaxial octocopter configuration was built and tested for autonomy. The size of this drone is less than 60 cm, allowing it to fit in all the accessible sewer sections in Barcelona. With approximately 11 minutes and 30 seconds of flight time during the test, its autonomy is satisfactory although should be improved. Moreover, an operating procedure of the system for inspection was introduced.

All in all, this thesis with its implementation has proved that using an aerial vehicle for an underground application is possible and advantageous.

Suggestion for future works

The result of the research and execution in this thesis is rather satisfactory. However, a lot of improvements can be made for a better implementation of the thesis. Some ideas of improving the inspection are listed below.

Firstly, Firstly, autonomous flight needs to be really implemented in the platform. Although this thesis has proposed the concept of completely autonomous flight, this needs to be implemented in the final product to take the full advantages of the technology.

Secondly, the incorporation of photogrammetry in the inspection needs to be studied. At present, this topic is only regarded as part of the payloads. In real application, this will be an important part of the inspection. It should be added that Lidar surveying for 3D reconstruction is also a promising direction. Nevertheless, a different Lidar sensor may be needed for this purpose as the one discussed in this thesis has quite short range.

Lastly, the drone platform needs to be further developed. The current flight time and lift capacity is acceptable although could be improved. This can be done by using higher capacity batteries and more powerful motors. Yet this will add more weight to the platform. For that reason more research needs to be done to find the best balance. Additionally, the platform needs a better casing to protect it from dust and water during its operation.

Acronyms

AC	Alternating current
AESA	Agencia Estatal de Seguridad Aérea
BCASA	Barcelona Cicle d/e l'Aigua, SA
BSD	Berkeley Software Distribution License
CERN	Conseil Européen pour la Recherche Nucléaire
DC	Direct Current
GNSS	Global Navigation Satellite System
GPS	Global Positioning System
GNU, GPL	General Public Licence
GUI	Graphical User Interface
IFOV	Instantaneous Field of View
IMU	Inertial Measurement Unit
Lidar, LiDAR, LIDAR	Light Detection and Ranging
LiPo	Lithium-Ion polymer Battery
POS	Position and Orientation System
PM	Precision Mode
PWM	Pulse-Width Modulation
RGBD	3D camera
SP	Speed Mode
TR One	TeraRanger One sensor

Bibliography

[1] D. Saurí and L. Palau-Rof, “Urban drainage in barcelona: From hazard to resource?,” *Water Altern.*, vol. 10, no. 2, pp. 475–492, 2017.

[2] “COMMON SANITARY SEWER SYSTEM PROBLEMS.” [Online]. Available: http://www.moperm.com/Resources/PW/PW03.pdf.

[3] “Trials to select a robot that will inspect the urban drainage network and the sewer system,” *Ajuntament de Barcelona*. [Online]. Available: http://ajuntament.barcelona.cat/lafabricadelsol/en/noticia/trials-to-select-a-robot-that-will-inspect-the-urban-drainage-network-and-the-sewer-system. [Accessed: 01-Mar-2018].

[4] “CHALLENGE BRIEF – RELATED TO THE ECHORD++ CALL FOR R&D PROPOSALS,” 2014. [Online]. Available: http://echord.eu/pdti/pdti-urban-robotics-sewer-inspection/. [Accessed: 02-Mar-2018].

[5] C. Weitkamp, *Lidar Range-Resolved Optical Remote Sensing of the Atmosphere*. Springer, 2005.

[6] T. Luo, R. Yuan, and Z. Wang, “Lidar-based remote sensing of atmospheric boundary layer height over land and ocean,” *Atmos. Meas. Tech.*, vol. 7, no. 1, pp. 173–182, 2014.

[7] P. Dong and Q. Chen, *LiDAR Remote Sensing and Applications*. CRC Press, 2017.

[8] A. Wehr and U. Lohr, “Airborne laser scanning - an introduction and overview,” *ISPRS J. Photogramm. Remote Sens.*, vol. 54, pp. 68–82, 1999.

[9] J. Shan and C. K. Toth, *Topographic Laser Ranging and Scanning: Principles and Processing*, Second. CRC Press, 2008.

[10] M.J.Westoby, J.Brasington, N.F.Glasser, M.J.Hambrey, and J.M.Reynolds, “‘Structure-from-Motion’ photogrammetry: A low-cost, effective tool for geoscience applications,” *Geomorphology*, vol. 179, 2012.

[11] S. P. Geopositioning, “NGA STANDARDIZATION DOCUMENT Light Detection and Ranging (LIDAR) Sensor Model Supporting Precise Geopositioning,” no. November, 2011.

[12] M. Ruffo *et al.*, “New infrared time of-flight measurement sensor for robotic platforms,” *IMEKO TC4 Int. Symp. Int. Work. ADC Model. Test.*, no. Figure 2, pp. 13–18, 2014.

[13] “Data sheet for XL-Maxsonar-EZ MB1200 High Performance Sonar Range Finder, MaxBotix Inc.”

[14] “Data sheet for SF01 Laser Range Finder, LightWare Optoelectronics.”

[15] “Data sheet for UTM 30LX, Hokuyo Automatic Co.”

[16] “Data sheet for TeraRanger V2, Terabee.”

[17] C. M. Simões, “Optimizing a Coaxial Propulsion System to a Quadcopter,” pp. 1–10, 2015.

Annex: TeraRanger One Connection to Pixhawk Autopilots

This annex presents the instruction manual showing how rangefinder TeraRanger One from Terabee is connected to Pixhawk flight controller through the I2C interface and how to setup PX4 or ArduPilot firmware to enable TeraRanger One sensor use. The manual can be found on Tera bee's website (www.terabee.com).

I. Compatibility

TeraRanger One sensor is compatible with PX4 from Flight Stack v1.6.5 onwards and APM ArduPilot from Copter v3.5.3 onwards.

II. Wiring Connection to Pixhawk

The wiring is slightly different between Pixhawk 2.1 and Pixhawk 1. The subsequent part will show both of them one after the other.

II.1. TeraRanger One wiring connection with Pixhawk 2.1

In order to wire TeraRanger One sensor to Pixhawk controller, we need an I2C (inter-integrated circuit) connector with DF13 connection shown in the following figure.

Figure 1: TeraRanger One sensor (1) and its I2C connector (2)

The I2C connector needs to be soldered to the power cable as follow:

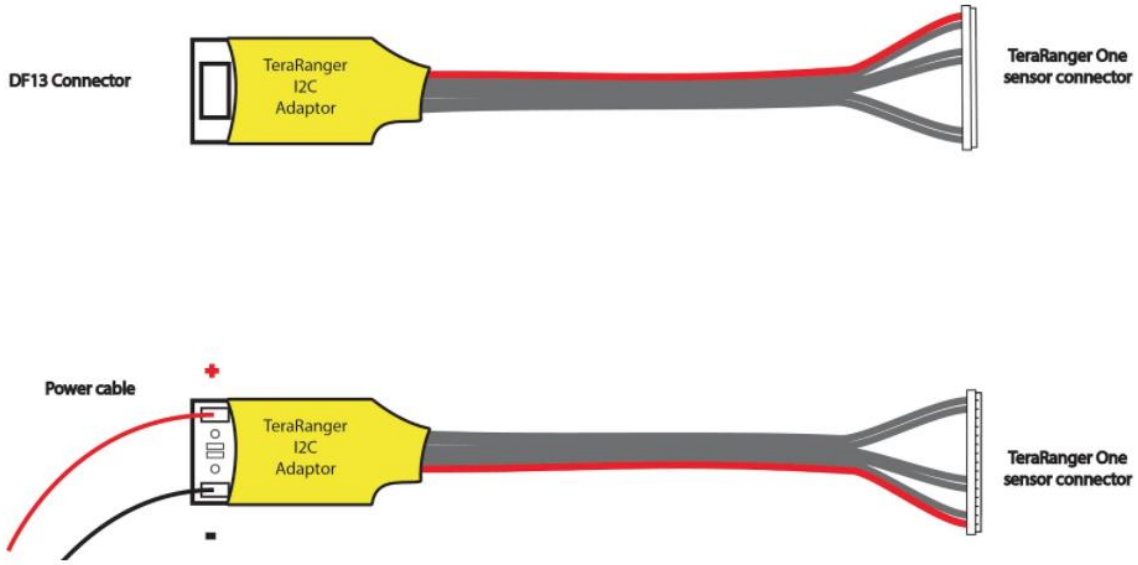

Figure 2: Soldering of power cable to TeraRange One I2C connector.

The I2C pin of Pixhawk 2.1 needs to be wired to TeraRange One pin as shown

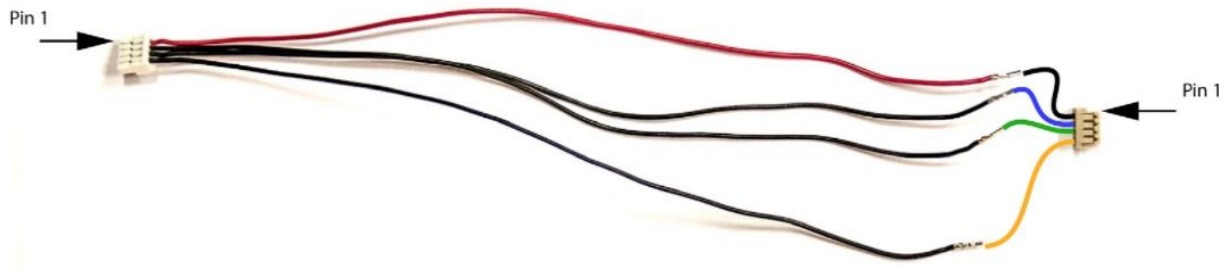

Figure 3: Soldering of TeraRange I2C adapter to Pixhawk 2.1 port pins

Table 1: Cable colors guide to connect TeraRange I2C Adapter to Pixhawk 2.1 I2C port

TeraRange I2C Adapter pins	Pixhawk 2.1 I2C port pins	Color
1 VCC	1 VCC	Orange
2 SCL	2 SCL	Green
3 SDA	3 SDA	Blue
4 GND	4 GND	Black

Finally, the TeraRange sensor can now be connected to Pixhawk 2.1 at the I2C port, as shown in the figure bellow.

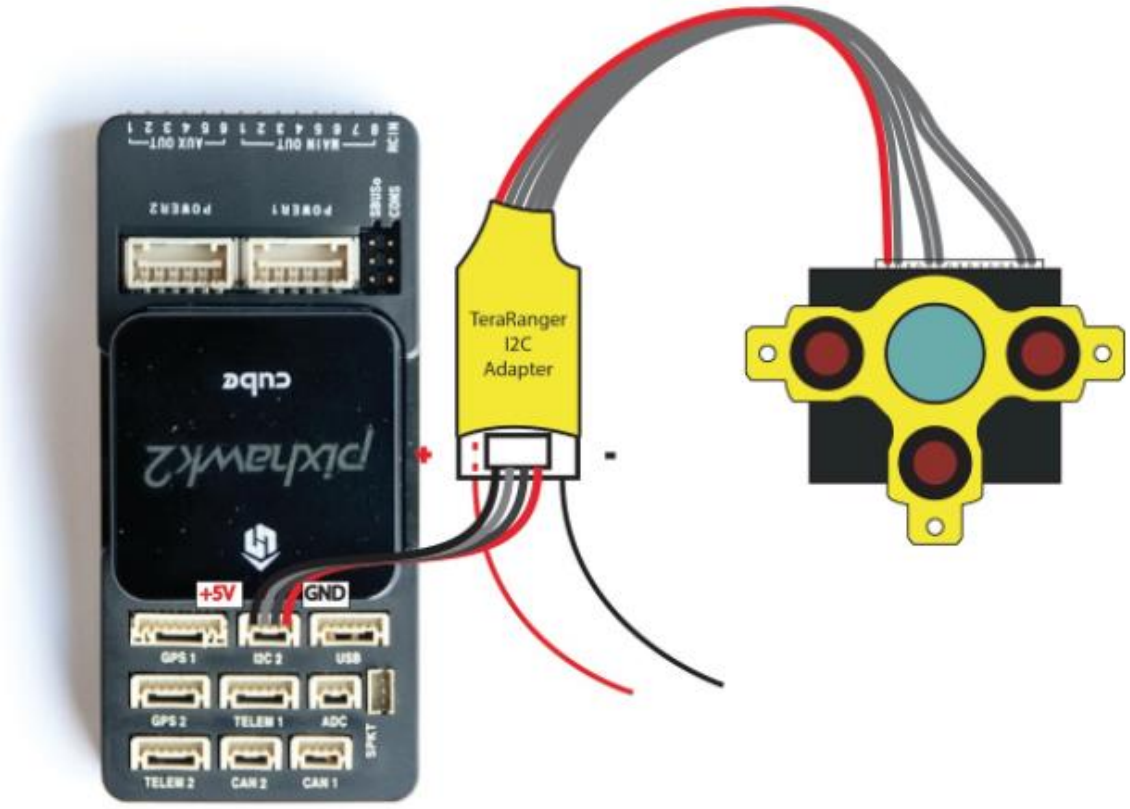

Figure 4: TeraRange sensor connected to Pixhawk 2.1

II.2. TeraRanger One wiring connection with Pixhawk 1

Similarly to the previous description, The I2C connector needs to be soldered to the power cable.

Next, the I2C adaptor of TeraRanger One is connected to Pixhawk 1 via a DF13 4S cable respecting the pins as described in the bellow table:

Table 2: Pin guide to connect TeraRange I2C adapter to Pixhawk 1 I2C port.

TeraRange I2C Adapter pins	Pixhawk I2C port pins
1 VCC	1 VCC
2 SCL	2 SCL
3 SDA	3 SDA
4 GND	4 GND

The final connection of TeraRanger One and Pixhawk 1 controller is shown in the figure bellow.

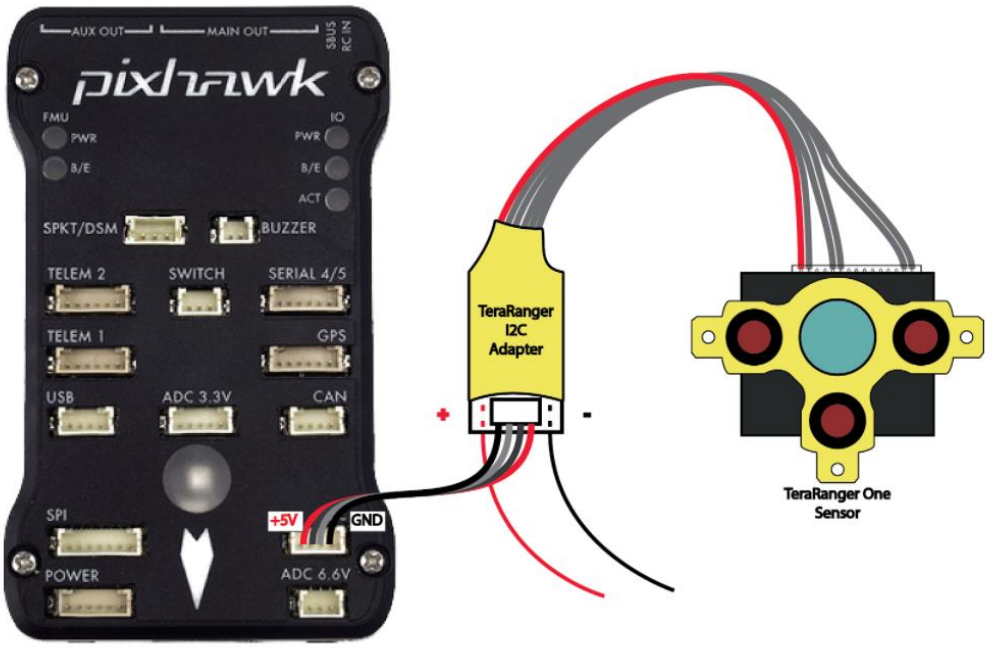

Figure 5: TeraRange sensor connected to Pixhawk 1

III. Setup the onboard firmware

We will use QGroundControl and Mission Planner to illustrate the setup on Ground Control Station (GCS).

III.1. Setup PX4 with QGroundControl

- Launch QGroundControl software

- Open Vehicle setup menu and go into the Firmware tab (unplug and replug autopilot if needed).

- Select the latest stable release of PX4 Flight Stack. Press the Ok button to flash the autopilot.

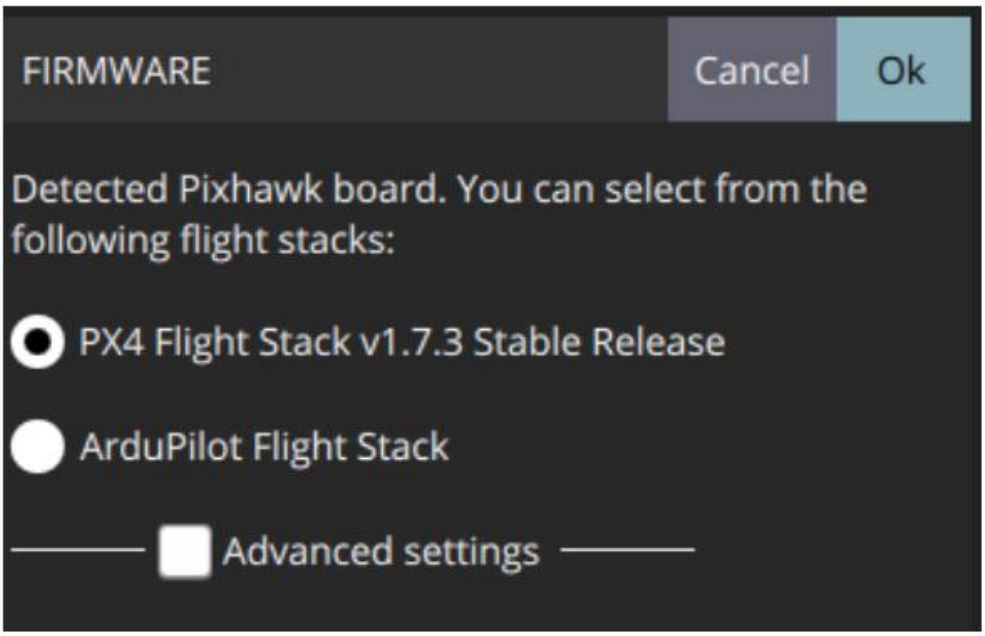

Figure 6: Select PX4 Flight Stack

- Go to Parameters/Sensor Enable

In the field SENS_EN_TRANGER select TeraRanger sensor type:

- TROne

Press Save to confirm.

Figure 7: Select TeraRanger sensor TROne

- After making sure the sensor is connected to the Pixhawk I2C port, reboot the autopilot.

- To verify that the sensor is operational open an Analyze Widget (Widgets/Analyze). From the list on the left hand side select; M1:DISTANCE_SENSOR.current_distance. The plot showing distance measurements should indicate that the sensor is working correctly.

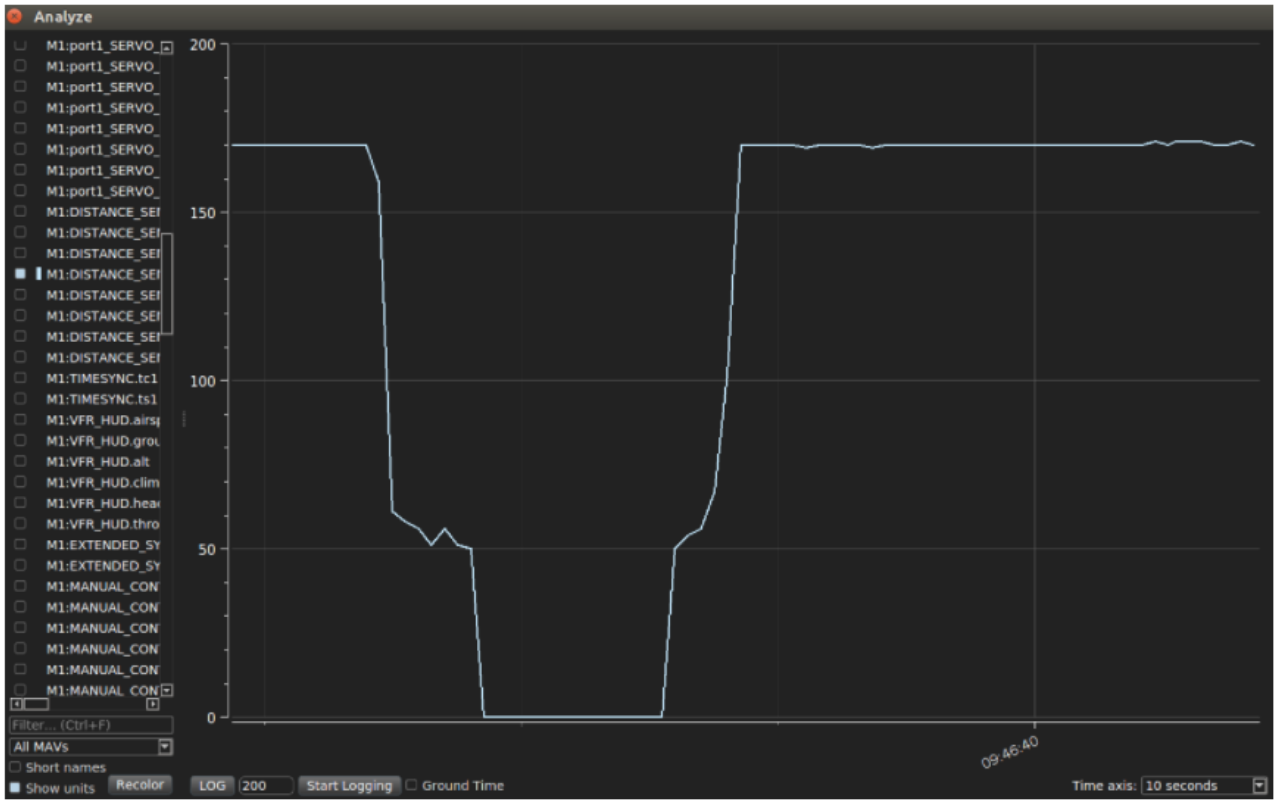

Figure 8: Example of distance measurements plot

III.2. Setup ArduCopter with QGroundControl

- Go to the Firmware tab on QGroundControl (reconnect autopilot in order to flash a new firmware). Select ArduPilot Flight Stack. In the dropdown menu select the latest version of MultiRotor – APM:Copter.

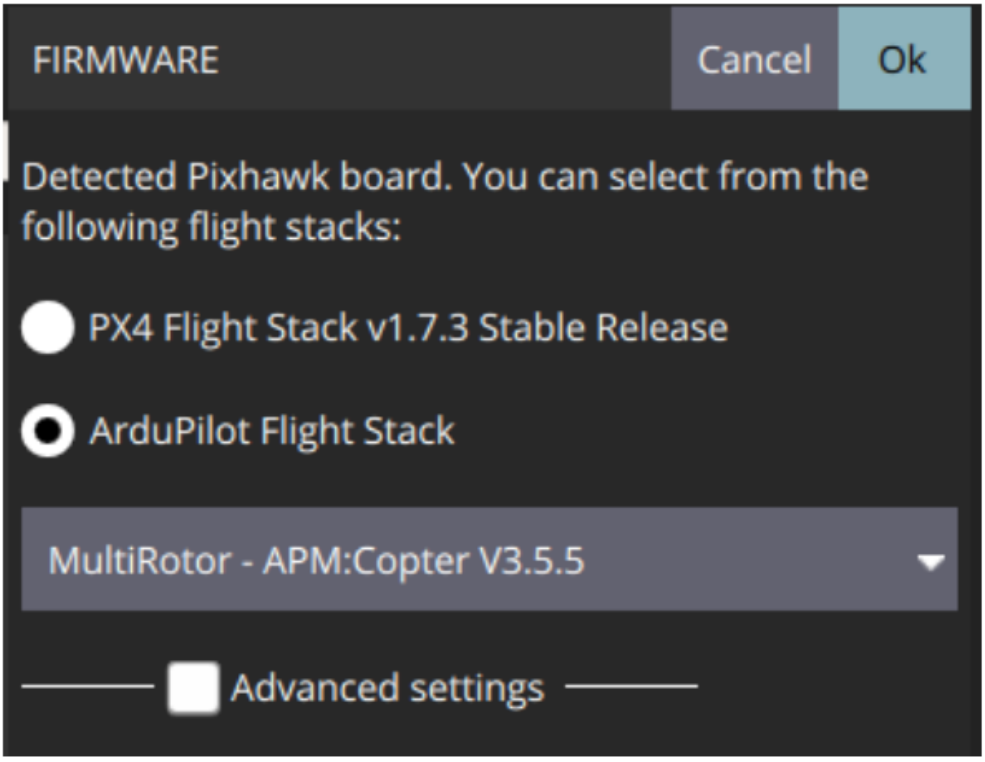

Figure 9: Select MultiRotor – APM: Copter of ArduPilot Flight Stack

- Go to Parameters/RNGFND and update the following fields:
  - RNGFND_TYPE : 14 / TrOneI2c / TeraRangerI2C (each of these values should work, but they might appear differently based on GCS software version.)
  - RNGFND_ADDR:
    - TR-One : 48
  - RNGFND_MIN_CM:
    - TR-One : 20
  - RNGFND_MAX_CM:
    - TR-One : 1400

After setting the values in these fields, reboot the autopilot.

-To verify that the sensor is operational open an Analyze Widget (Widgets/Analyze). From the list on the left hand side select; M1:DISTANCE_SENSOR.current_distance. The plot showing distance measurements should indicate that the sensor is working correctly.

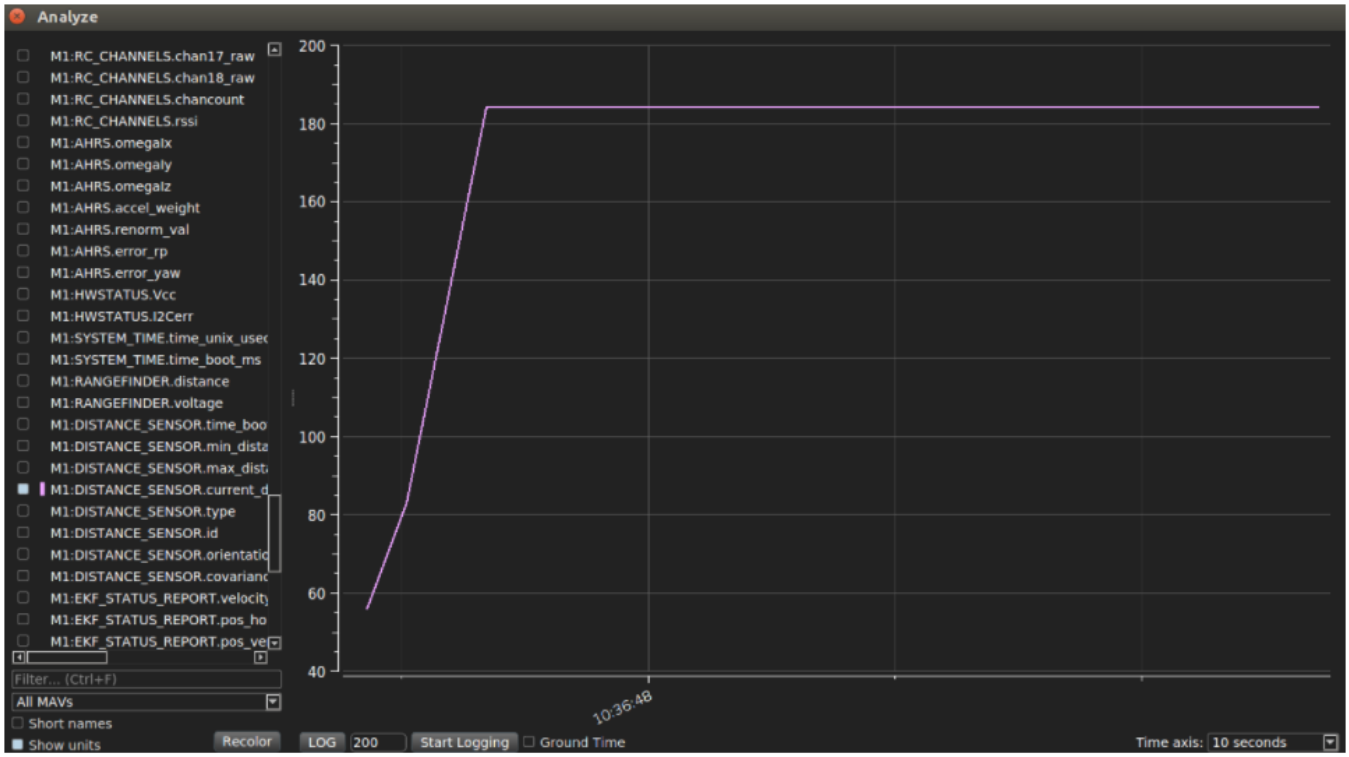

Figure 10: Example of distance measurements plot

III.3. Setup ArduCopter with APM Planner 2

- Open APM Planner. Go to Initial Setup, Instal Firmware and flash the latest firmware of ArduPilot.
- Click on USB device name on the right hand side and select the appropriate Serial Port and Baud Rate for your device and press the Connect button (Figure 11).

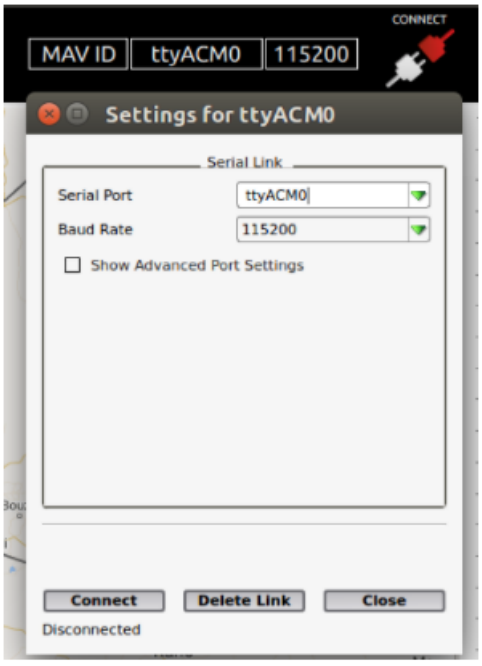

Figure 11: Select the appropriate Serial Port and Baud Rate

- Go to Parameters/RNGFND and update the following fields:
    - RNGFND_TYPE : 14 / TrOneI2c / TeraRangerI2C (each of these values should work, but they might appear differently based on GCS software version.)
    - RNGFND_ADDR:
        - TR-One : 48
    - RNGFND_MIN_CM:
        - TR-One : 20
    - RNGFND_MAX_CM:
        - TR-One : 1400

- Reboot the autopilot and select the GRAPHS tab. On the right hand side you should see the messages from the autopilot. From the list select; DISTANCE_SENSOR/current_distance:

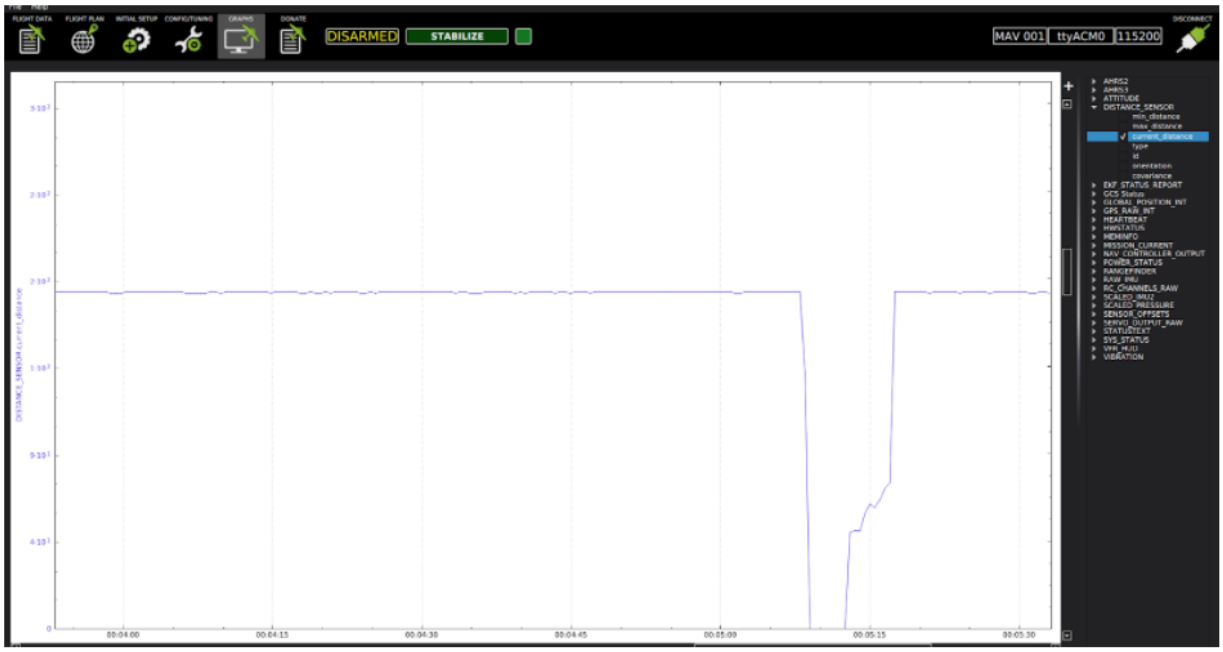

Figure 12: Example of distance measurements plot

III.4. Setup ArduCopter – Mission Planner

- Open Mission Planner. Go to Initial Setup, Instal Firmware and flash the latest firmware.

- Click on USB device name on the right hand side and select appropriate Serial Port and Baud Rate for your device and press the Connect button.

- Go to Parameters/RNGFND and update the following fields:

- RNGFND_TYPE : 14 / TrOneI2c / TeraRangerI2C (each of these values should work, but they might appear differently based on GCS software version.)
- RNGFND_ADDR:
  - TR-One : 48
- RNGFND_MIN_CM:
  - TR-One : 20
- RNGFND_MAX_CM:
  - TR-One : 1400

- Reboot the autopilot and select the Flight Data tab. On the left window you should see a quick tab with displayed value. Double click on one and check SonarRange. The distance is now displayed on the Quick flight data menu.

Figure 13: Example of distance is displaying on the Quick flight data menu.